High Power Laser Science and Engineering, (2024), Vol. 12, e74, 10 pages.
doi:10.1017/hpl.2024.49

HIGH POWER LASER SCIENCE AND ENGINEERING

RESEARCH ARTICLE

Kilowatt-level spectrum-programmable multi-wavelength fiber laser

Yanzhao Ke[1], Jiangming Xu[1], Jun Ye[1,2,3], Junhong He[1], Junrui Liang[1], Yang Zhang[1], Yidong Guo[1], Lei Du[1], Jinyong Leng[1,2,3], Pu Zhou[1], and Lei Si[1,2,3]

[1]*College of Advanced Interdisciplinary Studies, National University of Defense Technology, Changsha, China*

[2]*Nanhu Laser Laboratory, National University of Defense Technology, Changsha, China*

[3]*Hunan Provincial Key Laboratory of High Energy Laser Technology, National University of Defense Technology, Changsha, China*

(Received 9 May 2024; revised 9 July 2024; accepted 25 July 2024)

Abstract

This study demonstrates a kilowatt-level, spectrum-programmable, multi-wavelength fiber laser (MWFL) with wavelength, interval and intensity tunability. The central wavelength tuning range is 1060–1095 nm and the tunable number is controllable from 1 to 5. The wavelength interval can be tuned from 6 to 32 nm and the intensity of each channel can be adjusted independently. Maximum output power up to approximately 1100 W has been achieved by master oscillator power amplifier structures. We also investigate the wavelength evolution experimentally considering the difference of gain competition, which may give a primary reference for kW-level high-power MWFL spectral manipulation. To the best of our knowledge, this is the highest output power ever reported for a programmable MWFL. Benefiting from its high power and flexible spectral manipulability, the proposed MWFL has great potential in versatile applications such as nonlinear frequency conversion and spectroscopy.

Keywords: high-power fiber laser; multi-wavelength; spectrum programmable laser

1. Introduction

Recently, there has been an increasing interest in spectrum-programmable multi-wavelength fiber lasers (MWFLs) due to their various applications in laser sensing[1,2], nonlinear frequency conversion[3,4], wavelength division multiplexing communications[5], microwave generation[6], adaptive wavefront shaping[7], and so on[8]. In terms of the laser generation process, MWFLs can generally be categorized into two types: one utilizes nonlinear optical effects such as the four-wave-mixing effect[9] and stimulated Brillouin scattering[10] to achieve multi-wavelength lasing directly. MWFLs based on such nonlinear optical effects show advantages in terms of narrower laser linewidth and increasing laser line quantity. However, it is challenging to achieve flexible control of spectrum envelopes and wavelength intervals as the pump lasers and fiber characteristics greatly influence the nonlinear conversion process. At the same time, the other way is to use spectral filters, including the Mach–Zehnder interferometer[11,12], Fabry–Pérot filter[13], fiber grating[14–16], Sagnac fiber loop filter[17], Lyot filter[18,19], acousto-optic tunable filter (AOTF)[20], multimode interference filter (MMIF)[21] and spatial light modulator (SLM)-based wavelength selective switch (WSS)[22,23], to provide spectral filtering. With the recent development of spectral filtering devices, MWFLs utilizing such methods have evolved rapidly. However, most studies have focused on improving the stability and laser line quantity[24–27] of MWFLs, and few works have investigated the power scaling[28] and wavelength flexible manipulation[29]. Achieving high-power multi-wavelength operation is challenging due to wavelength competition and signal-to-noise ratio (SNR) degradation caused by nonlinear effects. These effects become more pronounced as power increases and wavelength intervals decrease. Various techniques have been proposed to suppress this competition, such as nonlinear amplification loop mirrors[30], nonlinear polarization rotation[31,32] and four-wave mixing (FWM)[33]. These methods introduce

Correspondence to: J. Xu and P. Zhou, College of Advanced Interdisciplinary Studies, National University of Defense Technology, Changsha 410073, China. Emails: jmxu1988@163.com (J. Xu); zhoupu203@163.com (P. Zhou)

wavelength-dependent loss to select the desired wavelengths. However, most filters provide a rectangular or periodic comb filtering spectrum[19,34], which limits the ability to manipulate the wavelengths flexibly.

In contrast to traditional methods, AOTFs have garnered significant attention as they are capable of providing quick and precise feedback of light waves without moving components involved. This unique characteristic makes AOTFs a promising candidate for achieving spectrum-programmable MWFLs. Although AOTFs have been successfully employed in various fields, such as laser spectroscopy[35], multi-spectral imaging[36] and mode-locked laser systems[37], their use in the construction of MWFLs has been relatively limited. In 2021, Yue *et al.*[38] reported central wavelength and relative intensity tuning capability of an AOTF-based ytterbium-doped fiber laser (YDFL). However, the maximum output power of this YDFL was limited to about 5 mW. In 2022, Li *et al.*[39] confirmed the potential of AOTF-based schemes to generate flattened multi-wavelength lasers at the dozen-watt level by a cladding-pump scheme and optimize the coupling ratio of the feedback loop to 10%, with the maximal output power of this YDFL increased to 15.7 W. Both studies by Yue *et al.*[38] and Li *et al.*[39] demonstrated the flexible tunability of the central wavelength, interval, intensity and laser line quantity. In 2023, Liang *et al.*[28] demonstrated a hundred-watt level AOTF-based scheme by reducing the ratio of feedback to 1%. In practical applications such as nonlinear frequency conversion, lasers with higher power and more flexible envelope tunability are usually preferred to realize gain design and improve conversion efficiency. At power levels exceeding the hundred-watt mark, the modest feedback intensity of 1% poses tunability concerns for the ring cavity. In addition, the hundred-watt output has approached the upper limits of certain fiber components, such as couplers. The secondary question involves how the spectrum evolves with varying power adjustments in the amplifier. Getting an understanding of this dynamic is essential for establishing optimal multi-pass feedback levels and for compensating gain disparities when scaling the MWFL's power. This, in turn, is key to achieving flexible spectral control.

In this study, a spectrum-programmable MWFL with kilowatt-level output power is demonstrated. We address the power scaling challenge by integrating a seed MWFL at the dozen-watt scale with a master oscillator power amplifier (MOPA) structure, thereby amplifying the output to the kilowatt range, an order of magnitude higher. Moreover, the system retains its flexible wavelength tuning capability. The tunability of the laser channel quantity, central wavelength, interval and intensity is achieved by using an AOTF as a programmable spectral filter. The laser line envelope can be further manipulated by balancing the amplifier gain and the seed laser. The MWFL seed laser is designed to have a maximum output power above 20 W, ensuring the safe operation of the ring cavity within a safe power range while providing enough optical signal for kilowatt power amplification. To the best of our knowledge, this is the highest output power ever reported for MWFLs, while exhibiting excellent spectrum reconfigurability.

2. Experimental setup

The experimental setup for the proposed MOPA structured spectrum-programmable MWFL is depicted in Figure 1, and is composed of a polarization-maintaining (PM) seed laser and a non-PM amplifier. The seed laser follows a standard ring cavity configuration made of all-PM fibers and devices. Two 976 nm laser diodes (LDs) are employed to pump the fiber laser via a $(2 + 1) \times 1$ PM signal-pump combiner. The pump laser is injected into a 6-m-long 10/125 μm PM Yb-doped fiber (YDF) with a core numerical aperture (NA) of approximately 0.075 and an average cladding absorption of approximately 5 dB/m at 976 nm. A fast-axis-blocked 90/10 coupler is utilized, and 90% of the light is extracted as high-power output. The remaining 10% of light is adjusted

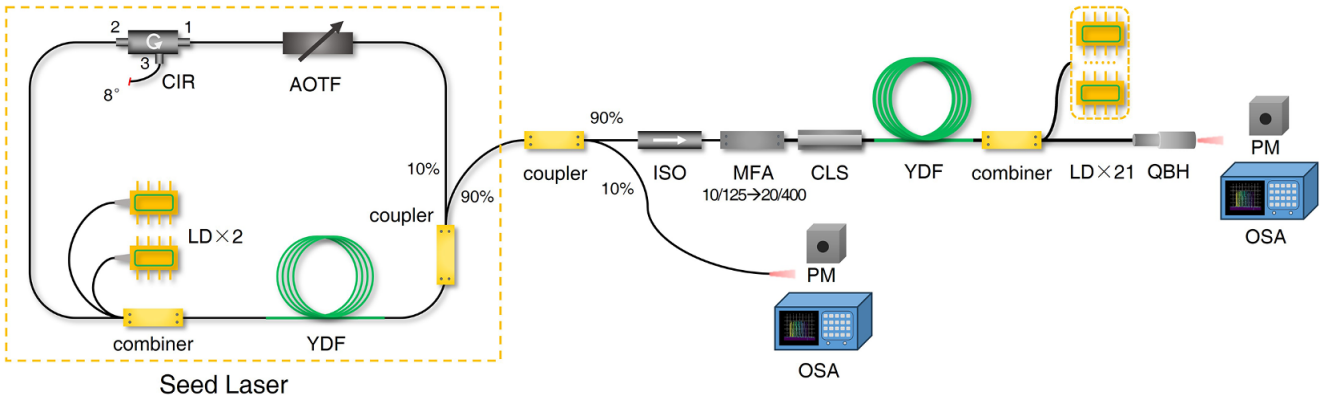

Figure 1. Experimental setup of the tunable MWFL. LD, laser diode; YDF, Yb-doped fiber; AOTF, acoustic optical tunable filter; CIR, optical circulator; ISO, optical isolator; MFA, mode field adaptor; CLS, cladding light stripper; QBH, quartz block head; PM, power meter; OSA, optical spectrum analyzer.

https://doi.org/10.1017/hpl.2024.49 Published online by Cambridge University Press

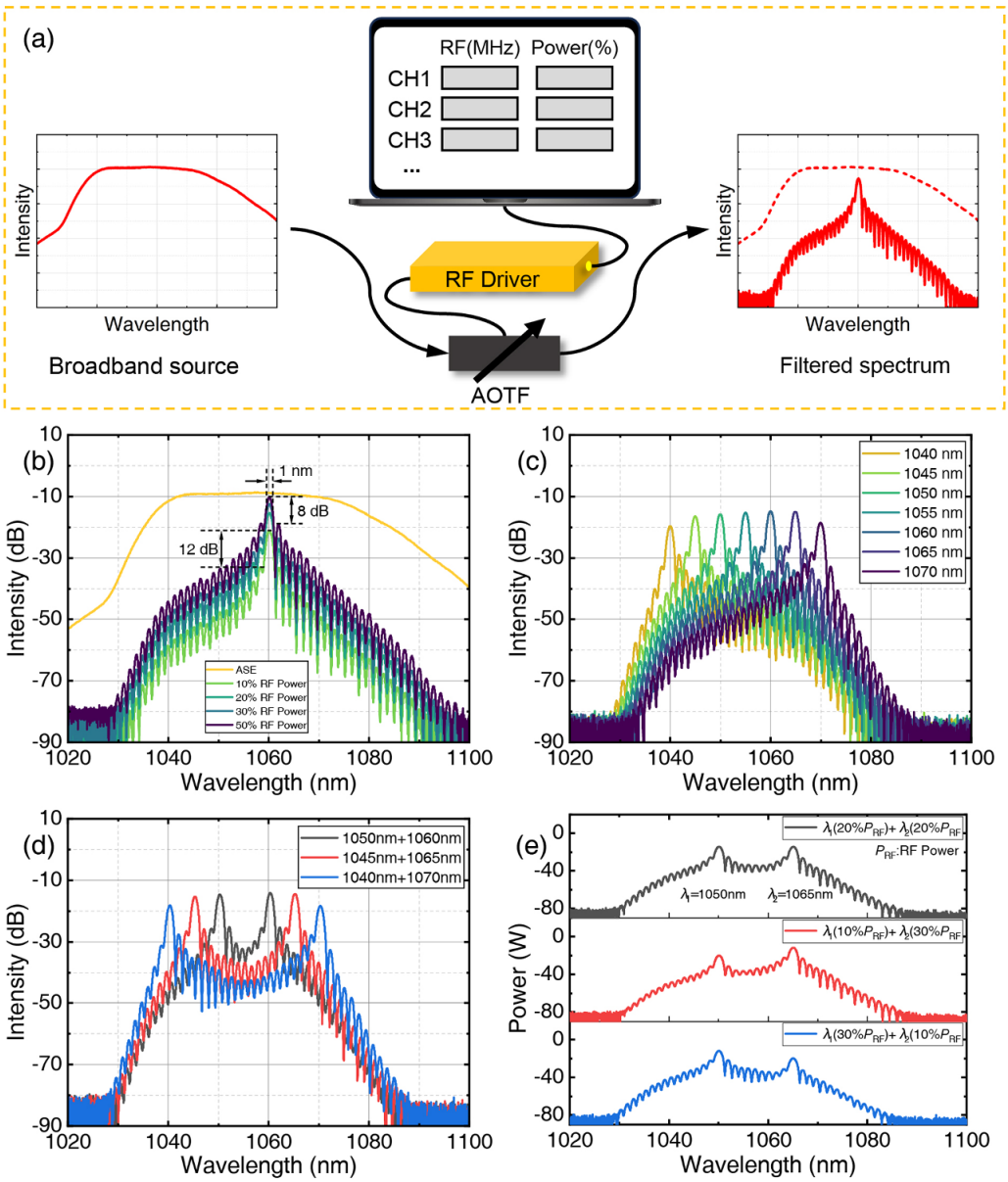

Figure 2. AOTF-based spectrum manipulation techniques. (a) Illustration of the AOTF's operational mechanism. (b) AOTF's transmission spectra under varying applied RF powers. (c) AOTF's transmission spectra with adjustable RF frequencies, highlighting the shift in the central wavelength. (d) Demonstration of wavelength spacing adjustability in AOTF's transmission spectra. (e) AOTF's transmission spectra for a dual-channel configuration with varied RF power to illustrate channel-specific control.

by a fast-axis-blocked AOTF and becomes feedback in the ring cavity. The AOTF is electrically driven by the applied radio frequency (RF) signals, which can be conveniently controlled by a computer. A fast-axis-blocked optical circulator is inserted within the loop following the AOTF to enforce unidirectional operation and to monitor and prevent harmful backward light. The light exiting the ring cavity is further divided by a PM 90/10 coupler. The primary portion, which is 90% of the light, is then amplified through a typical MOPA structure. The remaining 10% is used to monitor the power and spectrum of the seed laser. To isolate the backward light from the amplifier, a 10/125 μm optical isolator is spliced after the seed laser. A mode field adapter (MFA) with input and output fiber diameters of 10/125 and 20/400 μm, respectively, is then connected after the isolator. A backward pump structure is employed during the amplification, which consists of a 25-m-long 20/400 μm YDF and 21 LDs with a maximum pump power of more than 2 kW. In addition, a cladding light stripper (CLS) is spliced between the MFA and the YDF to filter out the residual pump light. Finally, a quartz block head (QBH) is used to output the high-power multi-wavelength lasing to free space. All the end facets are cleaved at an angle of 8° to suppress undesired backward reflection.

As shown in Figure 2(a), the AOTF achieves spectral tunability by applying an RF signal, with insertion loss

https://doi.org/10.1017/hpl.2024.49 Published online by Cambridge University Press

controlled by varying the RF signal power. The AOTF's designed tunable spectral range is 1000–1300 nm, but for this study its operational range is 1020–1110 nm. The AOTF's center wavelength corresponds directly to the RF signal frequency, achieving a resolution finer than 0.02 nm, exceeding that of the optical spectrum analyzer utilized in the current study. Each filtered wavelength's transmission through the AOTF is dictated by the RF power level. The pigtailed fiber's core and cladding diameters are 9 and 125 μm, respectively, with an NA of 0.085.

To demonstrate its filtering capabilities, we measured the AOTF using a broadband commercial amplified spontaneous emission (ASE) source, which maintains intensity flatness below 3.5 dB within the 1040–1075 nm band. In Figure 2(b), the AOTF's filtering spectrum at 1060 nm central wavelength varies with RF power level. The main peak exhibits a 3 dB linewidth of approximately 1.0 nm, accompanied by adjacent sidebands. Increasing RF power up to 50% of the RF driver's maximum capacity minimizes filtering loss to 2 dB. Beyond 50%, the main peak transmission plateaus, while sideband intensities increase. Spectral contrast between the main peak and sidebands starts at 12 dB at 10% RF power, decreasing to 8 dB at 50%.

Figure 2(c) illustrates the flexibility of the AOTF's central wavelength tuning through adjustments in the RF signal frequency. Figures 2(d) and 2(e) further demonstrate that the wavelength spacing and transmission profiles can be precisely controlled by varying the RF intervals and power, respectively. Within the oscillator, the influence of gain competition leads to linewidth narrowing of the main peak and the elimination of sidebands. Thus, we fine-tune the intensity levels of each channel, enabling precise spectral management of the MWFL system. Leveraging this characteristic, we can develop a spectrum-programmable multi-wavelength fiber seed laser by modulating the transmission intensity across various laser channels. Furthermore, the gain profiles of YDF amplifiers require pre-compensation of the seed laser to ensure attainment of the desired spectral envelope during the high-power amplification phase.

3. Results and discussion

3.1. Multi-wavelength operation seed laser

To begin with, we measured the central wavelength tunability of the multi-wavelength seed laser. Figure 3(a) displays the output power and backward power within the ring cavity when the pump power reaches 3.5 W, slightly above the lasing threshold. The output is measured at the 90% port of the 90/10 coupler, while the back power is measured at port 3 of the optical circulator. Benefiting from the one-to-one relation between RF and operating wavelength, the central wavelength tunability is accurately quantitative. We were able to achieve a continuous wavelength tuning range from 1030 to 1100 nm. However, for the edge of the tuning range, specifically the 1035 and 1100 nm, the backward ASE light is slightly higher. This may result in lower conversion efficiency from the LD to tunable laser and unstable feedback to the ring cavity. This situation becomes even more dangerous when the seed laser is injected into the amplification systems. Hence, we have chosen the central wavelength range of 1040–1095 nm for the amplification. After that, the pump power is then increased to 31.2 W, leading the power of each channel to vary from 20 to 22 W, and the 3 dB linewidth of each channel is around 0.3–0.4 nm, as presented in Figure 3(b).

In Figure 3(c), the operation of a multi-wavelength laser with two to five wavelengths is demonstrated. The intensity of each wavelength can be precisely adjusted without noticeable fluctuation in operation numbers 2–5. The 3 dB linewidths are 0.35 and 0.29 nm for the dual-wavelength output, 0.27, 0.4 and 0.49 nm for the tri-wavelength output, 0.34, 0.39, 0.31 and 0.29 nm for the quadra-wavelength output and 0.26, 0.27, 0.21, 0.22 and 0.36 nm for the penta-wavelength output. It is evident that as the number of wavelength bands increases, the spectral linewidth tends to decrease due to wavelength competition. We also checked the power stability of the proposed multi-wavelength seed laser, which was set to operate in single-wavelength (1080 nm), tri-wavelength (1070, 1080 and 1090 nm) and penta-wavelength (1050, 1060, 1070, 1080, and 1090 nm) modes. We monitored the output power for 1000 seconds, and Figure 3(d) shows the stability measurement results. There are almost no observable power fluctuations over the measured period. The normalized standard deviation (NSD) values for total output power were 4.84%, 6.61% and 6.65% for single-wavelength, tri-wavelength and penta-wavelength modes, respectively. The multi-wavelength operation's repeatability is evidenced by the spectral measurements conducted over a 30-minute period for both the tri-wavelength and penta-wavelength outputs, as illustrated in Figures 3(e) and 3(f). The tri-wavelength configuration exhibited an intensity fluctuation of approximately 0.7 dB, whereas the penta-wavelength configuration showed a higher deviation, reaching about 1.2 dB, attributed to the enhanced competition among wavelengths.

3.2. Single-wavelength output and central wavelength tuning with kilowatt-level power

Figure 4(a) depicts the kilowatt-level output spectra of varied central wavelengths, and the pump–power relationship is illustrated in Figure 4(b). After power amplification, the tuning ranges from 1060 to 1095 nm, and a maximal power of 1109 W is achieved. The output power decreases slightly with the wavelength, and the maximum value can be scaled to approximately 1110 W at 1060 nm while the minimum power is about 1035 W at 1095 nm. Considering the system safety under high-power conditions, a tuning operation with

https://doi.org/10.1017/hpl.2024.49 Published online by Cambridge University Press

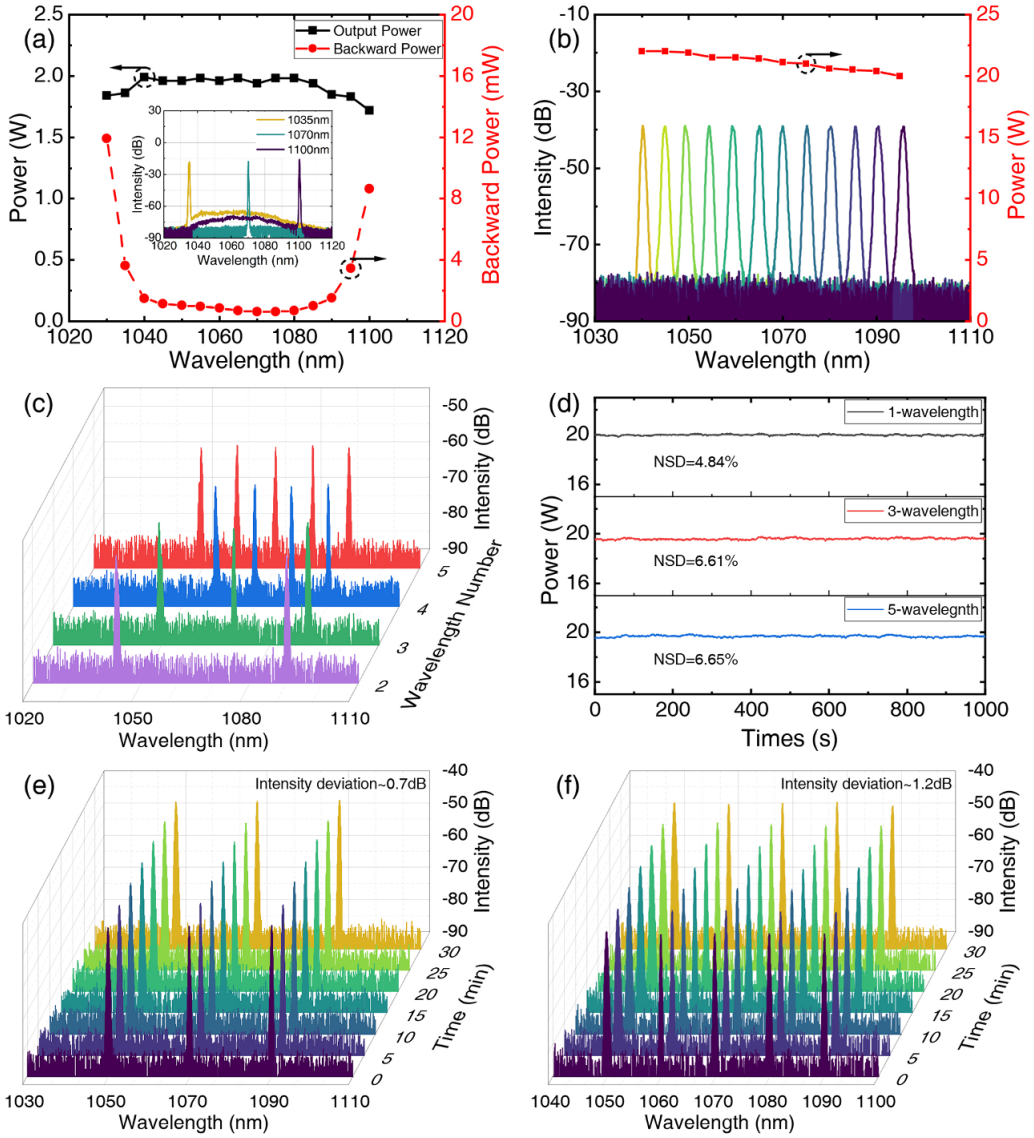

Figure 3. Power and spectrum characteristics of the multi-wavelength operating seed laser. (a) Output power and backward power at varied wavelengths and 3.5 W LD pump power. (b) Normalized spectrum and output power of varied single wavelength. (c) Spectra of multi-wavelength operation with channel numbers 2–5. (d) Power stability of one, three and five channels. (e) Spectral stability of tri-wavelength mode measured over 30 minutes. (f) Spectral stability of penta-wavelength mode measured over 30 minutes.

high power is absent. The long wave tuning is limited by the seed laser (as discussed in Section 3.1), and the tuning in the short wave is mainly limited by ASE, as shown in Figure 4(c). The 3 dB linewidths of the kW-level single wavelength are 2.1, 1.8, 1.7, 0.9, 2.2, 2.3, 2.3 and 1.6 nm, respectively.

In Figure 4(c), we can see the output spectra of a 1055 nm laser that has power amplification up to 1112 W. The ASE increases with the output power. This could be due to the longer gain fiber in the main amplifier reabsorbing the pump light. As the output power increases above 933 W, the stimulated Raman scattering (SRS) of 1055 nm (i.e., 1106 nm) grows rapidly due to the hybrid gain of SRS of the YDF. The ASE of the 1055 nm laser is strong and can potentially harm the amplifier. Therefore, the output wavelength is not adjusted to shorter waves to protect the amplifier. The spectrum evolution of a 1060 nm laser is showcased in Figure 4(d). The ASE during 1060 nm laser amplification is about 15 dB lower than that of the 1055 nm laser at the kilowatt level. However, the SRS induced by 1060 nm (around 1110 nm) grows gradually, benefiting from the ASE within the amplifier.

Figure 4(e) displays the spectrum evolution of a 1080 nm laser. It can be seen that the SRS threshold is about 914 W. On the other hand, Figure 4(f) shows the spectral evolution of a 1095 nm laser. As the output power grows to 313 W, the ASE becomes noticeable, and inter-mode four-wave mixing occurs[40].

https://doi.org/10.1017/hpl.2024.49 Published online by Cambridge University Press

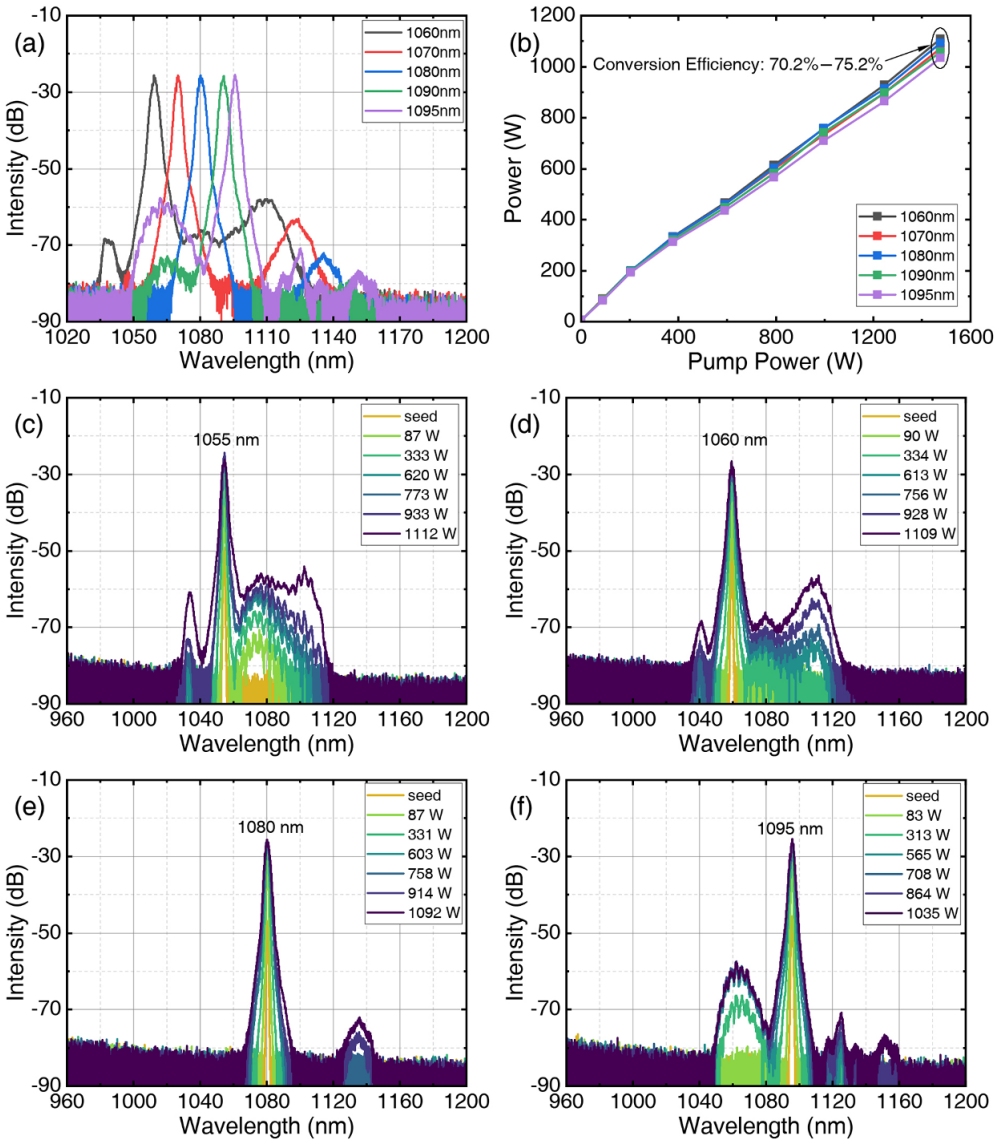

Figure 4. Spectra and power conversion efficiency of varied wavelengths at the kilowatt level. (a) Spectra of wavelengths from 1065 to 1095 nm at the kilowatt level. (b) Conversion efficiency from the pump to output power. (c) ASE of the 1055 nm laser. (d) Spectrum evolution of 1060 nm. (e) Spectrum evolution of 1080 nm. (f) Spectrum evolution of 1095 nm.

3.3. Multi-wavelength operation with interval, intensity, number and envelope tunability

The tunability of the MWFL's wavelength interval is studied under dual-wavelength operation. By adjusting the RF signals of two channels, dual-wavelength operation with interval tunability has been demonstrated. Figure 5(a) shows a set of dual-wavelength spectra with intervals ranging from 6 to 32 nm. The spectra consist of four different pairs of wavelengths, specifically 1077 and 1083 nm, 1075 and 1085 nm, 1070 and 1090 nm, and 1063 and 1095 nm. These pairs showcase a 3 dB linewidth that ranges from 1.2 to 2.6 nm. All the interval tuning modes operate at a power level higher than 1000 W, and the intensity difference is less than 1 dB. When the wavelength interval is less than 6 nm wide, the SNR will be less than 10 dB, which limits interval tuning. Achieving a flexible dual-wavelength output including 1060 nm presents a challenge due to the significantly lower gain of this wavelength within the amplifier. In addition, longer wavelengths, such as 1095 nm, may capitalize on the combined effect of the hybrid gain from the YDF and the SRS induced by the 1060 nm signal. Therefore, a wavelength shorter than 1063 nm is not demonstrated in this case. The output power exhibits a similar pump–power relationship to single-wavelength amplification.

In Figure 5(b), we demonstrate the ability to tune the intensity of the dual wavelength at constant intervals of 10 nm (specifically, 1070 and 1090 nm). The figure shows that the relative intensity can be flexibly adjusted within 0–10 dB. We also observed primary sideband wavelengths

https://doi.org/10.1017/hpl.2024.49 Published online by Cambridge University Press

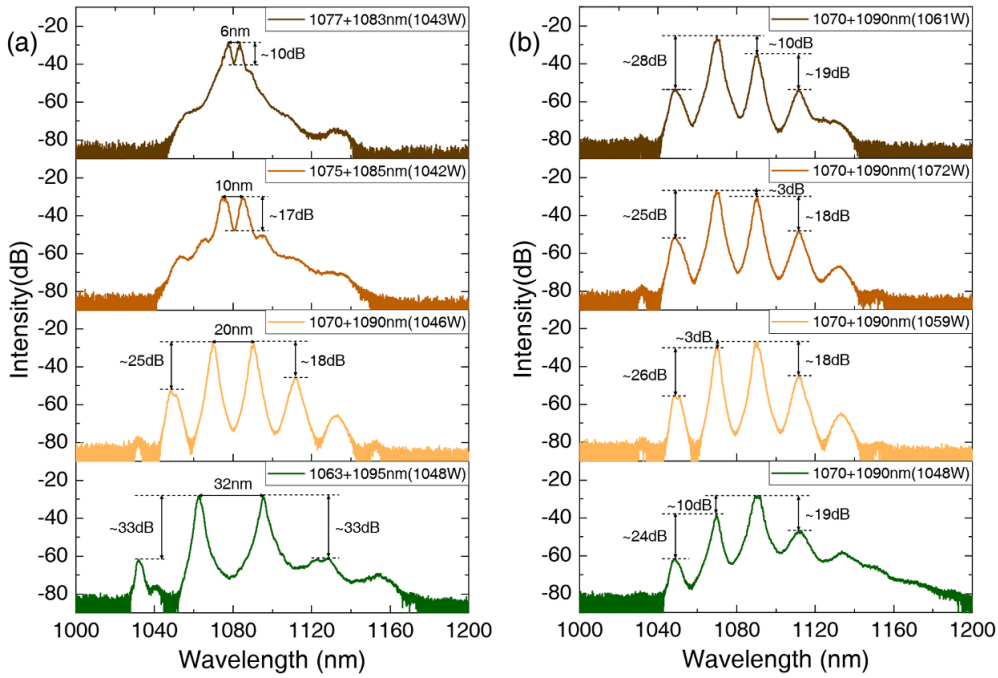

Figure 5. Interval and intensity tunability under dual-wavelength operation. (a) Interval tunability ranges from 6 to 32 nm. (b) Relative intensity can be flexibly adjusted within 0–10 dB.

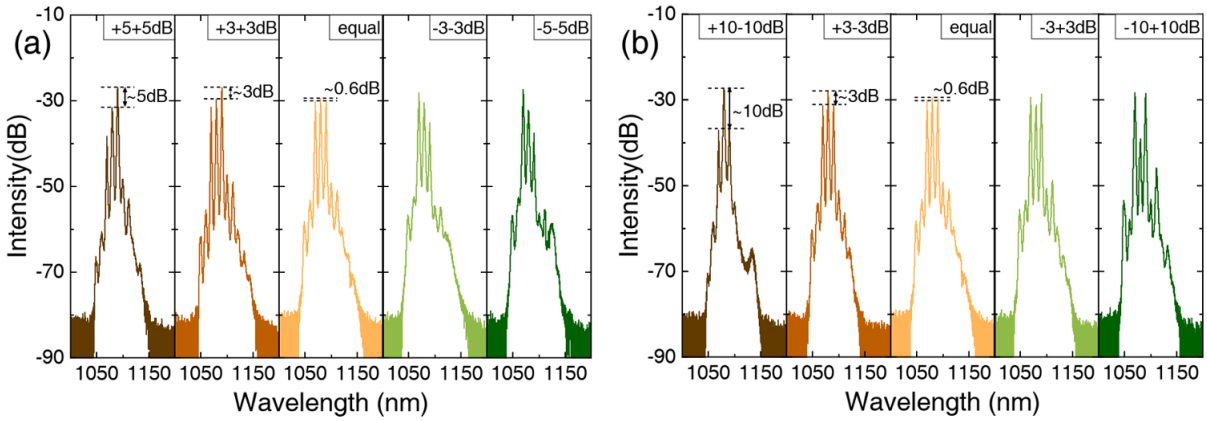

Figure 6. Tunability of the MWFL envelope. (a) Uphill and downhill shape. (b) Peak and basin shape.

at 1050 and 1110 nm, which is a result of the FWM effect of 1070 and 1090 nm. Both 1050 and 1110 nm wavelengths are located in the gain spectrum of YDF and can be amplified by the YDF, apart from the FWM effect. The 1110 nm wavelength has an intensity gap of around 18 dB compared to 1090 nm, and the 1050 nm wavelength has an intensity gap of around 25 dB in contrast to 1070 nm.

Furthermore, we have demonstrated the tunability of the MWFL envelope through flexible tri-wavelength intensity variation. Figure 6 displays spectra with tunable intensity at 1070, 1080, and 1090 nm. In Figure 6(a), an uphill and downhill envelope is showcased, while a peak and basin shape is displayed in Figure 6(b). The flattened tri-wavelength spectrum in Figure 6 has an output power of 1054 W. The intensity difference is limited to 0.6 dB, and the 3 dB linewidths of each channel are 1.2, 1.8 and 1.4 nm, respectively. By adjusting the amplitude of the corresponding RF signal channel and the resulting seed laser, the intensity of each wavelength can be independently tuned within approximately 10 dB. All the envelope-tuning modes operate at a power level higher than 1040 W. Such intensity and envelope tunability have enormous potential in multi-pump optimization for optical parametric amplifiers[41], gain flattening and special waveband design of multi-pumped Raman amplifiers[42,43], mode control through multimode optical fiber[23], and so on.

Figures 7(a) and 7(b) demonstrate an MWFL with wavelength quantities of four and five. In Figure 7(a), the central wavelengths are 1070, 1078, 1086 and 1094 nm, and the 3 dB linewidths of each channel measure 1.8, 1.6, 1.8 and

https://doi.org/10.1017/hpl.2024.49 Published online by Cambridge University Press

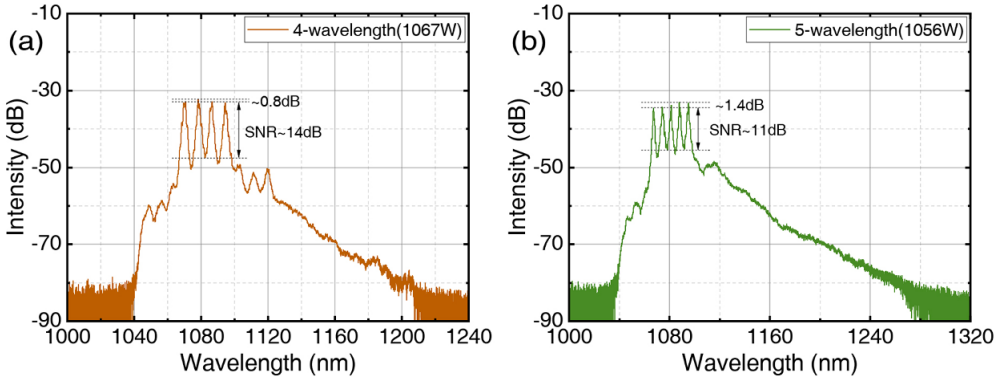

Figure 7. MWFL operation with wavelength quantities of four and five. (a) Spectrum of flattened four-wavelength output. (b) Spectrum of flattened five-wavelength output.

1.7 nm, respectively. The interval of the four wavelengths demonstrated here is 8 nm and the SNR is more than 14 dB. In Figure 7(b), the central wavelengths are 1067, 1074, 1081, 1088 and 1095 nm, and the 3 dB linewidths of each channel are recorded as 1.3, 1.6, 0.9, 1.6 and 1.5 nm, respectively. The interval of the five wavelengths demonstrated here is 7 nm and the SNR is about 11 dB, close to the limitation of the wavelength interval (6 nm interval and 10 dB SNR). During multi-wavelength operation, the presence of wavelength competition leads to a reduction in the linewidth when compared to single-wavelength operation. The intensity fluctuations of four and five wavelengths are successfully constrained within 0.8 and 1.4 dB, respectively.

It should be noted that in multi-wavelength operation, spectrum broadening occurs at both sides due to nonlinear optical effects, especially in the long wave direction part. The cut-off wavelength in the short wave of the broadened range direction is close to 1040 nm, which should be attributed to the FWM and self-phase modulation (SPM)[44] effects and limited by the reabsorption of YDF. The cut-off wavelength in the long wave increased with the channels, resulting from the complicated interaction of the above-mentioned effects and the SRS[45,46] effect. The spectrum span of the amplified five-wavelength laser has been spread from 1067–1095 to 1040–1270 nm, which is promising for supercontinuum generation when a random fiber amplifier structure is adopted[47]. Lasing with more channels is not examined here due to the wavelength competition and unsteady spectrum of the seed laser, which can be investigated and improved in further study.

3.4. Gain competition of laser lines

In the experimental setup, we detailed the approach for producing a flat multi-wavelength output in a ring oscillator and using an AOTF for precise spectral control. The YDF in the amplifier shows varying gains across wavelengths. Gain variation with power and nonlinear effects make quantitative analysis challenging. Knowing the gain characteristics is key for agile spectral tuning in high-power MWFLs. To facilitate the research, we started with uniform seed laser amplitudes and tracked the spectral evolution during power amplification.

Figure 8 displays how the spectra and spectral proportion change during the amplification of a seed laser with nearly equal intensity. The wavelengths used were set as 1060 + 1070, 1070 + 1080, 1080 + 1090 and 1070 + 1080 + 1090 nm. During amplification, the 1070, 1080 and 1090 nm wavelengths demonstrated higher gain compared to 1060 nm. Before the power increased to 1000 W, 1080 nm showed a higher gain than 1070 and 1090 nm. However, after the power exceeded 1000 W, the 1090 nm wavelength showed slightly higher intensity. Due to the generation of sideband wavelengths caused by nonlinear effects, the spectral proportion of the main wavelength slightly decreases as power increases.

It can be concluded that the peak gain is around 1080 nm at power levels below 1000 W. By adjusting the seed laser intensity at desired wavelengths, we can balance the gain disparity in the amplifier to achieve high-power target spectra. For example, to attain a flat dual-wavelength output at 1070 nm and 1080 nm, where 1080 nm has about 4 dB higher gain, we set the seed laser so that the 1080 nm wavelength is 4 dB less intense than the 1070 nm wavelength. However, multi-wavelength tuning including the 1060 nm wavelength is more difficult due to its significantly lower gain, requiring greater pre-compensation. As the laser power and wavelength number increase, nonlinear effects such as SRS and FWM make the energy distribution more complex. Studying spectral evolution through theories such as rate equations and nonlinear Schrödinger equations has become increasingly challenging and requires further investigation.

4. Conclusion

In summary, we have successfully developed a spectral programmable high-power MWFL by employing a MOPA

https://doi.org/10.1017/hpl.2024.49 Published online by Cambridge University Press

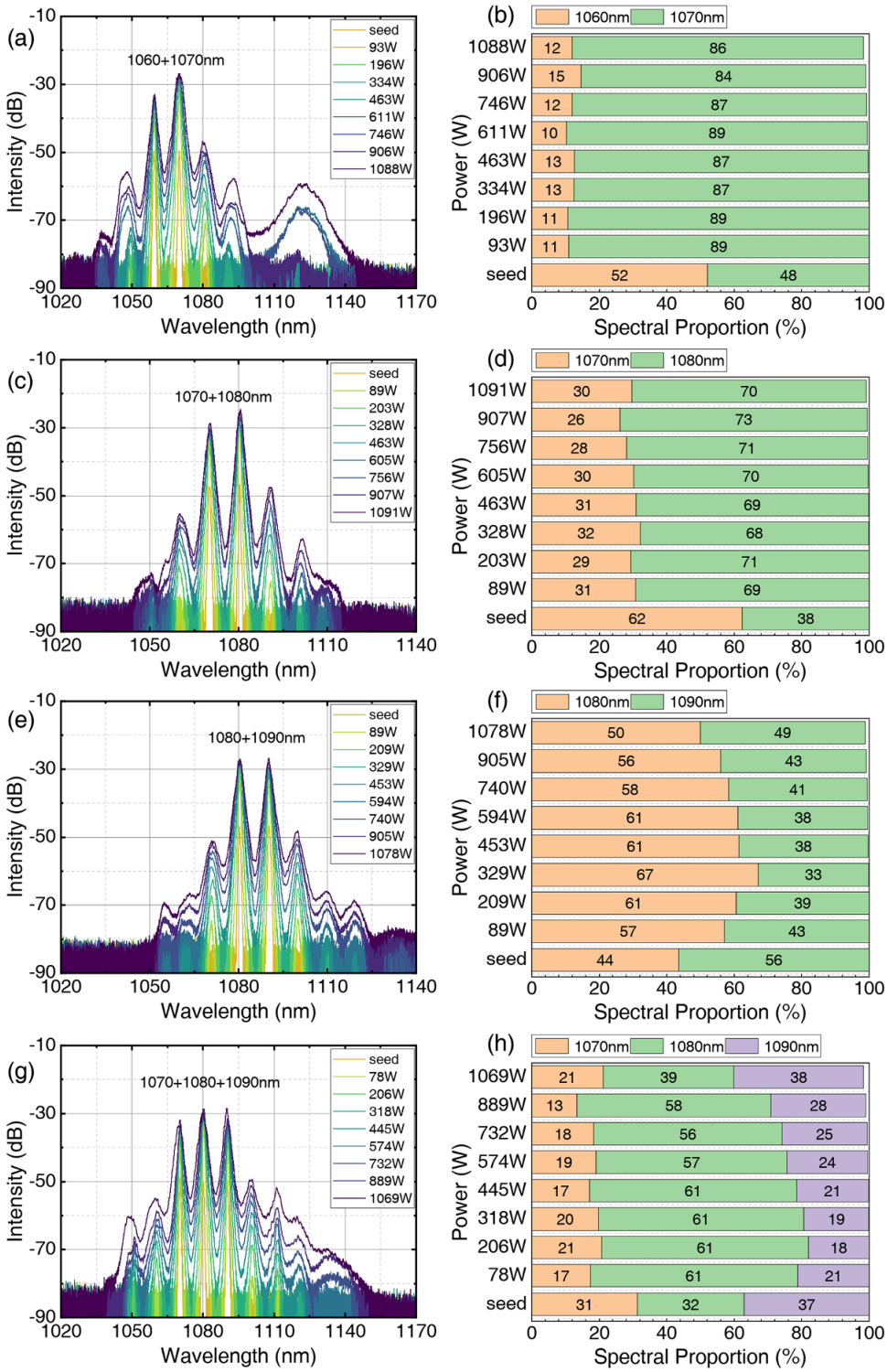

Figure 8. Spectral evolution of varied wavelength sets. (a), (b) 1060 + 1070 nm. (c), (d) 1070 + 1080 nm. (e), (f) 1080 + 1090 nm. (g), (h) 1070 + 1080 + 1090 nm.

structure. The maximal output power is 1109 W with an optical-to-optical conversion efficiency of 75.2%. An AOTF is adopted to control the spectrum and amplitude of the feedback signal. This enables us to independently adjust the channel number, wavelength, interval, intensity and envelope of the multi-wavelength output. The central wavelength can be continuously adjusted from 1060 to 1095 nm, and the channel number of the multi-wavelength output can be adjusted from one to five. In addition, the wavelength interval between two laser lines can be adjusted from 6 to 32 nm.

https://doi.org/10.1017/hpl.2024.49 Published online by Cambridge University Press

The power ratio of each channel can also be flexibly tuned. The wavelength tuning range is limited by ASE, while the channel number and wavelength interval are determined by the seed laser and nonlinear optical effects that induce spectrum broadening. We have also experimentally studied the amplifying gain of various wavelengths, offering significant insights into the scalable power potential of MWFLs and advancing the frontier of flexible spectral manipulation at the kilowatt level. To the best of our knowledge, this is the highest output power ever reported for an MWFL, and due to its flexible spectral manipulability, this laser can be used in many fields such as nonlinear frequency conversion.

Acknowledgements

This work was supported by the National Natural Science Foundation of China (No. 62305391), the Scientific Fund of the National University of Defense Technology (No. 22-061) and the Postgraduate Scientific Research Innovation Project of Hunan Province (No. CX20240126). The authors thank Sicheng Li for his helpful discussion about this work.

References

1. B. Zuo, M. Wang, B.-P. Lin, and H. Yang, Nat. Commun. **10**, 4539 (2019).
2. W. Yue, T. Chen, W. Kong, C. Mou, G. Huang, Z. He, and R. Shu, J. Lightwave Technol. **40**, 5995 (2022).
3. T. Chen, W. Yue, W. Kong, G. Huang, Z. He, and R. Shu, Opt. Lett. **48**, 6228 (2023).
4. H. Wu, W. Wang, B. Hu, Y. Li, K. Tian, R. Ma, C. Li, J. Liu, J. Yao, and H. Liang, Photonics Res. **11**, 808 (2023).
5. M. K. S. Al-Mashhadani, T. F. Al-Mashhadani, and H. H. Goktas, Opt. Commun. **451**, 116 (2019).
6. J. Shi, W. Sun, R. Chen, S. Yin, and X. Feng, Opt. Lett. **47**, 4861 (2022).
7. Y. Zhang, S. Wang, M. She, Y. Rao, and W. Zhang, Photonics Res. **11**, 20 (2023).
8. B. Han, Q. Cheng, Y. Tao, Y. Ma, H. Liang, R. Ma, Y. Qi, Y. Zhao, Z. Wang, and H. Wu, Laser Photonics Rev. **18**, 2400122 (2024).
9. A. W. Al-Alimi, M. H. Al-Mansoori, A. R. Sarmani, A. F. Abas, M. T. Alresheedi, and M. A. Mahdi, J. Lightwave Technol. **38**, 6648 (2020).
10. X. Geng, Y. Jiang, H. Gu, S. Luo, L. Li, and M. Sun, Opt. Commun. **531**, 129201 (2023).
11. Y. Guo, F. Yan, T. Feng, Q. Qin, Z. Bai, T. Li, W. Han, H. Zhou, and Y. Suo, Opt. Laser Technol. **145**, 107470 (2022).
12. J. D. Filoteo-Razo, J. C. Hernandez-Garcia, J. M. Estudillo-Ayala, O. Pottiez, D. Jauregui-Vazquez, J. M. Sierra-Hernandez, J. P. Lauterio-Cruz, C. M. Carrillo-Delgado, and R. Rojas-Laguna, Opt. Laser Technol. **139**, 106994 (2021).
13. A. Camarillo-Aviles, D. Jauregui-Vazquez, J. M. Estudillo-Ayala, E. Hernandez-Escobar, J. M. Sierra-Hernandez, O. Pottiez, M. Duran-Sanchez, B. Ibarra-Escamilla, and M. Bello-Jimenez, IEEE Photonics J. **11**, 7105307 (2019).
14. Y. Zhou, P. Gao, X. Zhang, P. Wang, L. Chen, and W. Gao, Chin. Opt. Lett. **17**, 010604 (2019).
15. L. Zhang, F. Yan, T. Feng, W. Han, B. Guan, Q. Qin, Y. Guo, W. Wang, Z. Bai, H. Zhou, and Y. Suo, Opt. Laser Technol. **136**, 106788 (2021).
16. B. Guo, X. Guo, L. Tang, W. Yang, Q. Chen, and Z. Ren, Chin. Opt. Lett. **19**, 071405 (2021).
17. Y. Zhang, J. Ye, X. Ma, J. Xu, J. Song, T. Yao, and P. Zhou, Opt. Express **29**, 5516 (2021).
18. J. Ye, Y. Zhang, J. Xu, J. Song, T. Yao, H. Xiao, J. Leng, and P. Zhou, Opt. Lett. **45**, 1786 (2020).
19. Q. Zhao, L. Pei, J. Zheng, M. Tang, Y. Xie, J. Li, and T. Ning, J. Lightwave Technol. **38**, 2428 (2020).
20. S. Li, J. Xu, J. Liang, J. Ye, Y. Zhang, X. Ma, J. Leng, and P. Zhou, Photonics Res. **11**, 159 (2023).
21. H. Wu, Q. Meng, J. Li, B. Han, Z. Wang, and Y. Rao, IEEE Access **6**, 39435 (2018).
22. M. A. F. Roelens, S. Frisken, J. A. Bolger, D. Abakoumov, G. Baxter, S. Poole, and B. J. Eggleton, J. Lightwave Technol. **26**, 73 (2008).
23. M. She, Z. Wang, Y. Zhang, A. Shi, and W. Zhang, IEEE Photonics Technol. Lett. **36**, 357 (2024).
24. H. Chen, X. Jiang, S. Xu, and H. Zhang, Chin. Opt. Lett. **18**, 041405 (2020).
25. Y. Chang, L. Pei, J. Wang, J. Zheng, T. Ning, J. Li, and C. Xie, Opt. Fiber Technol. **71**, 102894 (2022).
26. H. Hao, X. Zhou, M. Bi, M. Hu, G. Yang, Y. Lu, and T. Wang, Opt. Fiber Technol. **58**, 102296 (2020).
27. Z. Wang, H. Wu, M. Fan, Y. Li, Y. Gong, and Y. Rao, Opt. Express **21**, 29358 (2013).
28. J. Liang, J. Xu, Y. Zhang, J. Ye, S. Li, X. Ma, Y. Ke, J. Leng, and P. Zhou, J. Lightwave Technol. **42**, 882 (2024).
29. T. Huang, D. Zhang, S. Yoo, Q. Wei, R. Sidharthan, Z. Wu, B. Yan, C. Song, and Z. Cheng, Appl. Opt. **59**, 1163 (2020).
30. W. Peng, F. Yan, Q. Li, S. Liu, T. Feng, and S. Tan, Laser Phys. Lett. **10**, 115102 (2013).
31. Z. Zhang, L. Zhan, K. Xu, J. Wu, Y. Xia, and J. Lin, Opt. Lett. **33**, 324 (2008).
32. H. Ahmad and M. H. M. Ahmed, Opt. Eng. **58**, 046107 (2019).
33. Q. Zhao, L. Pei, M. Tang, Y. Xie, Z. Ruan, J. Zheng, and T. Ning, Opt. Fiber Technol. **54**, 102111 (2020).
34. J. Ye, C. Fan, J. Xu, H. Xiao, J. Leng, and P. Zhou, High Power Laser Sci. Eng. **9**, e55 (2021).
35. I. S. Khasanov, B. A. Knyazev, S. A. Lobastov, A. V. Anisimov, P. A. Nikitin, and O. E. Kameshkov, Materials **16**, 1820 (2023).
36. J. Fang, K. Huang, R. Qin, Y. Liang, E. Wu, M. Yan, and H. Zeng, Nat. Commun. **15**, 1811 (2024).
37. O. Henderson-Sapir, N. Bawden, M. R. Majewski, R. I. Woodward, D. J. Ottaway, and S. D. Jackson, Opt. Lett. **45**, 224 (2019).
38. W. Yue, T. Chen, W. Kong, Z. Ji, L. Yin, G. Huang, Z. He, and R. Shu, Opt. Lett. **46**, 1041 (2021).
39. S. Li, J. Xu, J. Liang, J. Ye, Y. Zhang, X. Ma, and P. Zhou, Opt. Lett. **47**, 4123 (2022).
40. L. Yin, Z. Han, H. Shen, and R. Zhu, Opt. Express **26**, 15804 (2018).
41. K. G. Tay, H. Pakarzadeh, A. Huong, N. Othman, and N. A. Cholan, Optik **253**, 168579 (2022).
42. D. Zibar, A. M. Rosa Brusin, U. C. de Moura, F. Da Ros, V. Curri, and A. Carena, J. Lightwave Technol. **38**, 736 (2020).
43. Y. Zhang, J. Xu, J. Liang, J. Ye, S. Li, X. Ma, Z. Pan, J. Leng, and P. Zhou, Front. Optoelectron. **17**, 1 (2024).
44. W. Liu, W. Kuang, L. Huang, and P. Zhou, Laser Phys. Lett. **12**, 045104 (2015).
45. G. P. Agrawal, *Nonlinear Fiber Optics*, 6th ed. (Academic Press, 2019), pp. 297–305.
46. C. Zhang, L. Xie, H. Li, B. Shen, X. Feng, M. Li, R. Tao, and J. Wang, IEEE Photonics J. **14**, 3016605 (2022).
47. L. Jiang, J. Wu, R. Song, Z. Chen, X. Zhu, F. Li, K. Li, H. Zhang, and J. Hou, High Power Laser Sci. Eng. **11**, e80 (2023).

https://doi.org/10.1017/hpl.2024.49 Published online by Cambridge University Press